
ProDAG: Projection-induced variational inference for directed acyclic graphs

Ryan Thompson*
University of New South Wales
CSIRO's Data61

Edwin V. Bonilla
CSIRO's Data61

Robert Kohn
University of New South Wales

Abstract

Directed acyclic graph (DAG) learning is a rapidly expanding field of research. Though the field has witnessed remarkable advances over the past few years, it remains statistically and computationally challenging to learn a single (point estimate) DAG from data, let alone provide uncertainty quantification. Our article addresses the difficult task of quantifying graph uncertainty by developing a variational Bayes inference framework based on novel distributions that have support directly on the space of DAGs. The distributions, which we use to form our prior and variational posterior, are induced by a projection operation, whereby an arbitrary continuous distribution is projected onto the space of sparse weighted acyclic adjacency matrices (matrix representations of DAGs) with probability mass on exact zeros. Though the projection constitutes a combinatorial optimization problem, it is solvable at scale via recently developed techniques that reformulate acyclicity as a continuous constraint. We empirically demonstrate that our method, ProDAG, can deliver accurate inference, and often outperforms existing state-of-the-art alternatives.

1 Introduction

A directed acyclic graph (DAG) has directed edges between nodes and no directed cycles, allowing it to represent complex conditional independencies compactly. DAGs play a central role in causal inference (Pearl, 2009) and consequently have found applications spanning a broad range of domains such as psychology (Foster, 2010), economics (Imbens, 2020), and epidemiology (Tennant et al., 2021). The literature on DAGs, dating back at least to the 1980s (Lauritzen and Spiegelhalter, 1988; Pearl, 1988), has recently witnessed a resurgence of interest due to a computational breakthrough by Zheng et al. (2018) that formulated a continuous characterization for the discrete notion of acyclicity. This breakthrough opened the door for scalable first-order algorithms that can learn DAG structures from datasets containing many more variables than previously considered feasible. We refer the reader to Vowels et al. (2022) and Kitson et al. (2023) for recent surveys of this ongoing work.

Unlike maximum likelihood approaches that only learn a point estimate DAG (Zheng et al., 2018; Bello et al., 2022; Deng et al., 2023), Bayesian approaches learn an entire posterior distribution over DAGs. This posterior quantifies graph uncertainty while acknowledging that the true DAG might be identifiable only up to its Markov equivalence class.² Uncertainty quantification also benefits tasks such as treatment effect estimation (Geffner et al., 2022) and experimental design (Annadani et al., 2023b). Most Bayesian approaches use a Gibbs-type prior based on a continuous acyclicity penalty (Geffner et al., 2022; Lorch et al., 2021; Annadani et al., 2021) or model DAGs in an augmented space where acyclicity is readily satisfied (Charpentier et al., 2022; Annadani et al., 2023a; Bonilla et al., 2024). While the former (Gibbs-type priors) do not guarantee an exact posterior over DAGs, the latter (augmented spaces) often require relaxations or cumbersome inference over discrete structures.

*Corresponding author. Email: ryan.thompson1@unsw.edu.au

²The Markov equivalence class is the set of DAGs that encode the same conditional independencies.

Our article introduces ProDAG, a Bayesian method for learning DAGs that departs from the approaches above. Leveraging the benefits of variational inference, ProDAG models the prior and variational posterior using new distributions having *exact support* on the space of DAGs. These DAG distributions are induced by mapping a continuous distribution \mathbb{P} onto the space of DAGs using a minimal distance projection. Consider a DAG represented by the weighted adjacency matrix $W \in \mathbb{R}^{p \times p}$ with entries w_{jk} that are nonzero if and only if there exists a directed edge from node j to node k . We induce a distribution over such matrices \tilde{W} , and hence over DAGs, using the data generating process

$$\tilde{W} \sim \mathbb{P}, \quad \lambda \sim \pi, \quad W = \text{proj}_\lambda(\tilde{W}), \quad (1)$$

where $\lambda \geq 0$ is a parameter governing the graph’s sparsity (number of active edges) with prior π and

$$\text{proj}_\lambda(\tilde{W}) := \arg \min_{W \in \text{DAG}, \|W\|_{\ell_1} \leq \lambda} \frac{1}{2} \|\tilde{W} - W\|_F^2 \quad (2)$$

is the projection of $\tilde{W} \in \mathbb{R}^{p \times p}$ onto the set of ℓ_1 constrained acyclic matrices.³ We prove this projection is a measurable mapping with a unique solution, yielding valid probability distributions. The key quality of these distributions is that they place probability mass on exact zeros, a necessity for sampling DAGs. Any sample drawn from such a distribution is a DAG with probability one.

Inspired by recently developed continuous DAG characterizations (e.g., [Zheng et al., 2018](#)), we reformulate the combinatorial optimization problem (2) as an equivalent continuous optimization problem that can be solved in parallel on a GPU. An analysis of the optimization problem’s Karush-Kuhn-Tucker conditions yields its gradients, meaning we differentiate through the projection and learn the distributions’ parameters. We use these results in a variational framework by forming the prior and variational posterior using the new distributions, enabling scalable Bayesian DAG learning. Our framework accommodates DAGs represented as linear and nonlinear structural equation models (SEMs), making our approach suitable for problems and data of varying complexity. Experiments on synthetic and real data demonstrate that our approach often delivers more accurate inference than existing methods for DAG learning. Our toolkit for ProDAG is open-sourced on [GitHub](#).

2 Related work

As mentioned, existing approaches for Bayesian inference on DAGs broadly fall into two categories: (1) regularization-based methods that include a continuous acyclicity penalty via a Gibbs-type prior in the variational objective (e.g., [Annadani et al., 2021](#); [Lorch et al., 2021](#); [Geffner et al., 2022](#)), and (2) state-augmentation methods that, e.g., place a prior over the graph’s topological ordering (e.g., [Cundy et al., 2021](#); [Charpentier et al., 2022](#); [Bonilla et al., 2024](#)). The node-potential augmentation of [Annadani et al. \(2023a\)](#) is closely related to the latter category. See also [Wang et al. \(2022\)](#) and [Deleu et al. \(2023\)](#) for approaches based on probabilistic circuits and generative flow networks. Our approach differs by designing a prior and approximate posterior directly over DAGs without modeling the (discrete) topological ordering and without using a penalty that does not place mass on zeros.

More broadly, our paper complements the literature on computational methods for point estimate DAG learning. The seminal paper of [Zheng et al. \(2018\)](#), which introduced the NOTEARS method, cleverly exploited the correspondence between the number of cycles in a matrix and the trace of that matrix’s power. A similar connection is now known to hold for other continuous functions and is exploited by methods such as DAGMA ([Bello et al., 2022](#)), which we utilize in this work, as well as those of [Ng et al. \(2020\)](#), [Yu et al. \(2021\)](#), and [Gillot and Parviainen \(2022\)](#). These approaches that use continuous characterizations of acyclicity are appealing in that they scale to large graphs and can be augmented with discrete combinatorics ([Manzour et al., 2021](#); [Deng et al., 2023](#)) if required. Though not pursued here, our projection onto DAG space is also amenable to discrete techniques.

Finally, though distributions over DAGs via projection is a seemingly new idea, others have previously used projections to construct distributions over non-graphical structures. [Xu and Duan \(2023\)](#) designed a distribution over sparse regression coefficients by projecting a vector drawn from a continuous distribution onto the ℓ_1 ball. They illustrated several computational advantages of their distribution as a prior in a Hamiltonian Monte Carlo (HMC) framework over classical spike-and-slab priors and prove that the resulting posterior enjoys the minimax concentration rate. [Xu et al. \(2023\)](#)

³The norm $\|W\|_{\ell_1} := \|\text{vec}(W)\|_1$.

extend this work to general proximal mappings with HMC, which includes the convex ℓ_1 projection as a special case. While our approach projects matrices onto the ℓ_1 ball, we also impose acyclicity, giving rise to a nonconvex combinatorial problem that does not constitute a proximal mapping.

3 Projection-induced distributions

3.1 Characterization

To recap the introduction, we induce a distribution over weighted acyclic adjacency matrices W as $W = \text{proj}_\lambda(\tilde{W})$, where proj_λ is defined in (2), $\tilde{W} \sim \mathbb{P}$ is a continuous matrix, and $\lambda \sim \pi$ bounds the ℓ_1 norm of W . Since acyclic graphs have no self-loops (i.e., W always has a zero diagonal), we can take \mathbb{P} to be any continuous distribution over the off-diagonal elements of \tilde{W} (e.g., a multivariate Gaussian), with the diagonal elements fixed as zero. The matrix \tilde{W} can thus be interpreted as the weighted adjacency matrix of a *simple directed graph*, with the projection removing all cycles.⁴

Besides removing cycles, the projection maps \tilde{W} onto an ℓ_1 ball of size λ . This part of the projection is necessary for sampling parsimonious graphs. It is not hard to see that without this constraint, the projection would return the densest possible acyclic graph with $(p^2 - p)/2$ edges.⁵ The advantage of constraining W to an ℓ_1 ball, compared with modeling \tilde{W} as a Laplace distribution, is that it gives probability mass on exact zeros beyond that already given by the acyclicity constraint. It is known that Laplace distributions do not concentrate on zero except at their mode (Park and Casella, 2008).

The resulting distribution $p(W)$ can be understood as a mix of continuous components and exact zeros. To elaborate, first observe that the nonzeros in W may be indexed by a sparsity pattern $S \in \{0, 1\}^{p \times p}$ (i.e., an unweighted acyclic adjacency matrix). The nonzeros are then given by W_S , where W_S is the restriction of W to S . Because the ℓ_1 constraint shrinks the nonzeros towards zero, the continuous W_S is a transformation f_λ of \tilde{W}_S , i.e., $W_S = f_\lambda(\tilde{W}_S)$, where f_λ is implicitly given by the projection. This mixture interpretation suggests an interesting representation of $p(W)$:

$$p(W) \equiv \sum_{i=1}^m p(W_{S_i} | S_i) p(S_i) = \sum_{i=1}^m p(f_\lambda(\tilde{W}_{S_i}) | S_i) p(S_i),$$

where S_1, \dots, S_m is the finite collection of all acyclic adjacency matrices. To reiterate, the distributions $p(f_\lambda(\tilde{W}_S) | S)$ and $p(S)$ on the right-hand side are *implicitly* defined by the projection. Though this representation is conceptual, it highlights that $p(W)$ forms a distribution over acyclic adjacency matrices S without explicitly having to model the discrete, high-dimensional probability mass function $p(S)$. Moreover, as we soon show, the projection can be reformulated as a continuous optimization problem, meaning it is unnecessary to deal with discreteness when sampling from $p(W)$.

3.2 Properties

One might ask if $p(W)$ is a valid distribution. Theorem 1 addresses this question in the affirmative by showing that the projection is almost surely unique and measurable. The proof is in Appendix A.

Theorem 1. *Let \tilde{W} be endowed with a continuous probability measure. Then it holds:*

1. *Projection (2) is unique almost surely with respect to the measure on \tilde{W} ; and*
2. *Projection (2) is measurable with respect to the measure on \tilde{W} .*

Theorem 1 states that, for continuous $\tilde{W} \sim \mathbb{P}$, the function $\text{proj}_\lambda(\tilde{W})$ is uniquely defined and measurable. This result implies that a projection-induced distribution is a valid distribution since a measurable function g applied to a random variable z produces a well-defined random variable $g(z)$.

⁴Simple directed graphs have no self-loops and, at most, one directed edge between any pair of nodes.

⁵An exception is the degenerate case where some off-diagonal elements of \tilde{W} are already zero.

3.3 Graph sparsity

To sample graphs W with a consistent number of edges, the distribution π of λ can be specified as a Dirac delta distribution concentrated on a point $\alpha \geq 0$ yielding the desired sparsity level:

$$\pi_\alpha(\lambda) = \delta(\lambda - \alpha).$$

Alternatively, to sample graphs of varying complexity, π can be specified as a distribution over $\lambda \geq 0$. For example, π can be taken as an exponential distribution parameterized by its mean $\alpha \geq 0$:

$$\pi_\alpha(\lambda) = \frac{\exp(-\lambda/\alpha)}{\alpha}, \quad \lambda \geq 0.$$

This specification of π allows for graphs with varying sparsity over the edges but primarily favors sparser (parsimonious) graphs over denser graphs for smaller values of α . The mean α of λ can be determined using expert domain knowledge or empirically calibrated on an available validation set.

4 Scalable projections

4.1 Continuous reformulation

To facilitate scalability, we reformulate the combinatorial projection (2) as an *equivalent* continuous optimization problem. This recharacterization is based on recent work (Zheng et al., 2018; Bello et al., 2022) showing that for certain functions $h(W)$ an important equivalence relationship holds:

$$h(W) = 0 \iff W \in \text{DAG}.$$

Bello et al. (2022) showed that for all matrices $W \in \mathbb{W} := \{W \in \mathbb{R}^{p \times p} : \rho(W \circ W) < 1\}$, where ρ is the spectral radius and \circ is the Hadamard product, the function $h(W) := -\log \det(I - W \circ W)$ (DAGMA) has this property. This function attains the value zero if and only if there are no cycles in W , and thus, its level set at zero exactly corresponds to the set of DAGs. Though it is a nonconvex function, it is continuous and differentiable in W . We can thus rewrite projection (2) equivalently as

$$\text{proj}_\lambda(\tilde{W}) = \arg \min_{W \in \mathbb{W}, h(W)=0, \|W\|_{\ell_1} \leq \lambda} \frac{1}{2} \|\tilde{W} - W\|_F^2. \quad (3)$$

As we show next, it is possible to (a) solve this projection at scale using only first-order methods and (b) analytically evaluate the gradients of this projection for gradient-based posterior learning.

4.2 Algorithm

To solve projection (3), we use a two-step alternating projection that produces a solution on the intersection of sets. Step one projects \tilde{W} onto the set of acyclic matrices, yielding a matrix \hat{W} . Step two projects \hat{W} onto the ℓ_1 ball, yielding the final output W that remains acyclic but is further sparse.

For the acyclicity projection, we use a path-following algorithm similar to Bello et al. (2022). This algorithm reformulates the problem by shifting the acyclicity constraint into the objective function:

$$\min_{W \in \mathbb{W}} f_\mu(W; \tilde{W}) := \frac{\mu}{2} \|\tilde{W} - W\|_F^2 + h(W). \quad (4)$$

Here, $\mu \geq 0$ is a coefficient taken along a sequence $\mu^{(1)} > \mu^{(2)} > \dots > \mu^{(T)}$. The path-following algorithm solves (4) at $\mu = \mu^{(t+1)}$ by using the solution at $\mu = \mu^{(t)}$ as an initialization point. The limiting solution as $\mu \rightarrow 0$ is guaranteed to satisfy the acyclicity constraint $h(W) = 0$ (Lemma 6, Bello et al., 2022). Algorithm 1 summarizes this procedure.

Algorithm 1: Solver for acyclicity projection

input : $\tilde{W} \in \mathbb{R}^{p \times p}$, $\lambda \geq 0$, $W^{(0)} \in \mathbb{W}$, $\mu^{(1)} > \dots > \mu^{(T)} \geq 0$

for $t = 0, 1, \dots, T - 1$ **do**

Initialize W at $W^{(t)}$ and set

$$W^{(t+1)} \leftarrow \arg \min_{W \in \mathbb{W}} f_{\mu^{(t+1)}}(W; \tilde{W}) \quad (5)$$

end

output : $\hat{W} = W^{(T)}$

We take $\mu^{(1)} = 1$, $\mu^{(t+1)} = \mu^{(t)}/2$, $T = 10$, and $W = 0 \in \mathbb{W}$, which work well in our experiments. The inner optimization problem (5) is amenable to gradient descent. The gradient of the objective function readily follows from the gradient of h , given by $\nabla h(W) = 2(I - W \circ W)^{-1} \circ W$.

For the ℓ_1 projection, we use an efficient (non-iterative) algorithm given by [Duchi et al. \(2008\)](#), which soft-thresholds the elements of the weighted adjacency matrix \hat{W} that is output by Algorithm 1. The soft-thresholding produces the final matrix W , a solution to the original projection (3).

4.3 Gradients

In many Bayesian learning frameworks, including our variational framework, it is necessary to compute gradients. In our case, this computation is complicated by the presence of the projection since we need its gradients with respect to \tilde{W} and λ . Though it is technically possible to differentiate through our algorithms using autograd, it is practically infeasible due to Algorithm 1 being iterative.

As it turns out, one can analytically evaluate the gradients via the implicit function theorem by differentiating the Karush-Kuhn-Tucker (KKT) conditions of the projection that implicitly define W as a function of \tilde{W} and λ . Theorem 2 presents these gradients. The proof is in Appendix B.

Theorem 2. *Let $W = (w_{jk}) \in \mathbb{R}^{p \times p}$ be the output of projection (3) applied to the matrix $\tilde{W} = (\tilde{w}_{jk}) \in \mathbb{R}^{p \times p}$ with sparsity parameter $\lambda > 0$. Let $\mathcal{A} := \{(j, k) : w_{jk} \neq 0\}$ be the set of active edge weights. Then, if the ℓ_1 constraint is binding, the gradients of w_{jk} with respect to \tilde{w}_{jk} and λ are*

$$\frac{\partial w_{jk}}{\partial \tilde{w}_{qr}} = \begin{cases} \delta_{jk}^{qr} - \frac{\text{sign}(w_{qr}) \text{sign}(w_{jk})}{|\mathcal{A}|} & \text{if } (j, k) \in \mathcal{A} \\ 0 & \text{otherwise} \end{cases} \quad \text{and} \quad \frac{\partial w_{jk}}{\partial \lambda} = \begin{cases} \frac{\text{sign}(w_{jk})}{|\mathcal{A}|} & \text{if } (j, k) \in \mathcal{A} \\ 0 & \text{otherwise,} \end{cases}$$

where $\delta_{jk}^{qr} := 1[(j, k) = (q, r)]$ and $|\mathcal{A}|$ is the cardinality of \mathcal{A} . Otherwise, if the ℓ_1 constraint is non-binding, the gradients are

$$\frac{\partial w_{jk}}{\partial \tilde{w}_{qr}} = \begin{cases} \delta_{jk}^{qr} & \text{if } (j, k) \in \mathcal{A} \\ 0 & \text{otherwise} \end{cases} \quad \text{and} \quad \frac{\partial w_{jk}}{\partial \lambda} = 0.$$

Theorem 2 indicates that the Jacobian is sparse and has nonzeros only in positions corresponding to the surviving elements in W . In the binding case, where the ℓ_1 constraint has a shrinkage effect, the value of the nonzeros depends on the size of the active set \mathcal{A} (the number of nonzero edges). In the non-binding case, where the ℓ_1 constraint imparts no shrinkage, all nonzero components equal one. Importantly, Theorem 2 indicates that only the projection’s output W is needed to evaluate the gradients; no additional computations are required. This result is highly useful for posterior learning since it means that a backward pass through the model demands virtually no further overhead cost.

[Thompson et al. \(2024\)](#) presented a result related to Theorem 2 in which they provided the gradients of a DAG projection for contextual learning. Their gradients differ slightly from those here because their sparsity constraint is different. The gradients relating to λ were not considered in their work.

5 Posterior learning

5.1 Variational inference

Suppose we have data $X \in \mathbb{R}^{n \times p}$, containing n observations on the variables $x \in \mathbb{R}^p$. Let $p(W)$ be a prior distribution over the weighted adjacency matrix W , taken here to be a projection-induced distribution. The conditional likelihood $p(X | W)$ is given by the linear SEM $x = W^\top x + \epsilon$, where $\epsilon \in \mathbb{R}^p$ is stochastic noise. Our task is to infer the posterior distribution $p(W | X)$. In general, this exact posterior is analytically intractable. Moreover, though our distribution admits a computationally convenient sampling algorithm, it is taxing to learn the posterior via traditional Bayesian approaches (e.g., Markov chain Monte Carlo) due to it being high-dimensional. To this end, we use variational inference to approximate the posterior (see [Blei et al., 2017](#)), leading to our method ProDAG.

Variational inference optimizes the parameters of an approximate posterior $q_\theta(W)$ such that it is nearest to the true posterior $p(W | X)$ in Kullback-Leibler (KL) divergence. Like the prior, the approximate posterior is taken here to be a projection-induced distribution. However, as discussed

later, performing variational inference on W alone is challenging because the projection is non-invertible. In other words, multiple unconstrained \tilde{W} can project to the same constrained (DAG) W . Towards this end, we focus on learning the joint posterior over both W and \tilde{W} . The joint posterior does not suffer from non-invertibility because for any given W , the associated \tilde{W} is also observed.

Let $p(\tilde{W}, W | X)$ be the true joint posterior and let $q_\theta(\tilde{W}, W)$ be the variational joint posterior. Since W is a deterministic function of \tilde{W} , the variational joint posterior is the product of the variational marginal posterior $q_\theta(\tilde{W})$ and a Dirac delta function: $q_\theta(\tilde{W}, W) = q_\theta(\tilde{W})\delta(W - \text{proj}_\lambda(\tilde{W}))$. The marginal $q_\theta(\tilde{W})$ can be any continuous distribution, e.g., a multivariate Gaussian. The variational parameters θ then contain means and covariances. Choosing $q_\theta(\tilde{W})$ is the same as choosing \mathbb{P} in (1).

5.2 Evidence lower bound

As in standard variational inference, we proceed by maximizing the evidence lower bound (ELBO):

$$\text{ELBO}(\theta) = \mathbb{E}_{q_\theta(\tilde{W}, W)}[\log p(X | \tilde{W}, W)] - \text{KL}[q_\theta(\tilde{W}, W) \parallel p(\tilde{W}, W)]. \quad (6)$$

The first term on the right-hand side of (6) is the expectation of the log-likelihood under the variational posterior. Since the log-likelihood depends only on \tilde{W} through W , this term simplifies to

$$\mathbb{E}_{q_\theta(\tilde{W}, W)}[\log p(X | \tilde{W}, W)] = \mathbb{E}_{q_\theta(W)}[\log p(X | W)].$$

To estimate this expectation, we sample DAGs from $q_\theta(W)$ and evaluate the log-likelihood on these samples. To sample from $q_\theta(W)$, we need only sample from $q_\theta(\tilde{W}, W)$ and discard \tilde{W} . The second term on the right-hand side of (6) is the KL divergence between the variational posterior $q_\theta(\tilde{W}, W)$ and the prior $p(\tilde{W}, W) = p(\tilde{W})\delta(W - \text{proj}_\lambda(\tilde{W}))$. Since W is a deterministic function of \tilde{W} , it is not too difficult to see that the KL divergence between the joint posterior and prior is equal to the KL divergence between the marginal posterior and prior on \tilde{W} . Hence, the second term also simplifies as

$$\text{KL}[q_\theta(\tilde{W}, W) \parallel p(\tilde{W}, W)] = \text{KL}[q_\theta(\tilde{W}) \parallel p(\tilde{W})].$$

Provided that $q_\theta(\tilde{W})$ and $p(\tilde{W})$ are chosen from distributional families with closed-form density functions (e.g., multivariate Gaussian distributions), this term is amenable to analytical evaluation. The gradients of Gaussians and other (more complex) distributions for \tilde{W} are accommodated in the ELBO using the well-known reparameterization trick (see, e.g., Kingma and Welling, 2014).

The challenge, mentioned earlier, of learning the marginal posterior of W alone arises due to the KL divergence appearing in (6). If we instead focus on the marginal posterior, the divergence term in (6) is between $q_\theta(W)$ and $p(W)$. With some work, one can show that the divergence between these terms involves the divergence between the (unknown) prior and posterior conditional distributions of \tilde{W} given W (since W is non-invertible in \tilde{W}). In any case, this issue is avoided in the joint posterior.

6 Nonlinear DAGs

6.1 Structural equation model

All our developments so far assume a linear SEM. However, our approach also accommodates nonlinear SEMs of the form $x = f(x) + \varepsilon$, where $f : \mathbb{R}^p \rightarrow \mathbb{R}^p$ is a nonlinear function with an acyclic Jacobian matrix. Acyclicity of the Jacobian matrix is necessary because $\partial f_k(x)/\partial x_j \neq 0$ indicates an edge exists from node j to node k . A standard choice of the function f is a neural network structured as $f(x) = (f_1(x), \dots, f_p(x))$, where $f_k(x)$ feedforward sub-network that models node k .

Let $\omega = (\omega_1, \dots, \omega_p)$ be a p -tuple of neural network weights corresponding to f_1, \dots, f_p . Denote by $\omega_k^h \in \mathbb{R}^{p \times d}$ the restriction of the k th network's weights ω_k to the first hidden layer, where d is the number of neurons in that layer. If the j th row of ω_k^h , denoted $\omega_{jk}^h \in \mathbb{R}^d$, is a zero vector (i.e., $\|\omega_{jk}^h\|_2 = 0$), then $\partial f_k(x)/\partial x_j = 0$ and no edge exists from node j to node k . Hence, we can enforce acyclicity on the Jacobian of $f(x)$ by enforcing acyclicity on the $p \times p$ matrix $W(\omega) := [\|\omega_{jk}^h\|_2]$.

6.2 Prior and posterior

In the nonlinear context, we induce a DAG distribution over *all* weights ω of the neural network as

$$\tilde{\omega} \sim \mathbb{P}, \quad \lambda \sim \pi, \quad \omega = \text{proj}_\lambda(\tilde{\omega}),$$

where \mathbb{P} is a continuous distribution over the weights. This data generating process yields a *fully Bayesian* neural network with every layer having a prior over its weights. The projection here modifies our earlier projection to now seek the weights ω nearest to $\tilde{\omega}$ such that $W(\omega)$ is acyclic and sparse:

$$\text{proj}_\lambda(\tilde{\omega}) := \arg \min_{W(\omega) \in \mathbb{W}, h(W(\omega))=0, \|W(\omega)\|_{\epsilon_1} \leq \lambda} \frac{1}{2} \sum_{k=1}^p \|\tilde{\omega}_k - \omega_k\|_F^2. \quad (7)$$

The matrix $W(\omega)$ that characterizes the constraints in (7) is a function only of the *first* hidden layer weights. Hence, the projection only modifies those weights and leaves the weights of other layers untouched. Though the weights on the input layer are significantly more numerous than in the linear case (d times as many weights), the projection can be reduced to a simpler problem that is no more complex than the linear case. Proposition 1 presents this result. The proof is in Appendix C.

Proposition 1. *Let $\tilde{\omega}$ be a tuple of neural network weights and let $\tilde{\omega}_{jk}^h$ be the vector of weights for the j th input to the first hidden layer of the k th output. Define the matrix \tilde{W} elementwise as $\tilde{w}_{jk} = \|\tilde{\omega}_{jk}^h\|_2$ and let W be the projection of \tilde{W} in (3). Then projection (7) is solved by taking $\omega_{jk}^h = \tilde{\omega}_{jk}^h w_{jk} / \tilde{w}_{jk}$ for $j, k = 1, \dots, p$ and leaving the remaining layers’ weights unmodified.*

Proposition 1 states that we need only project the matrix \tilde{W} constructed from $\tilde{\omega}$ to obtain the weights ω for an acyclic neural network $f(x)$. Consequently, the nonlinear setting requires no new algorithms.

Performing posterior inference for the neural network weights ω within our variational framework requires no major modifications. The only change required is to re-express the ELBO in terms of ω :

$$\text{ELBO}(\theta) = \mathbb{E}_{q_\theta(\omega)}[\log p(X | \omega)] - \text{KL}[q_\theta(\tilde{\omega}) \parallel p(\tilde{\omega})],$$

where the variational parameters θ now parameterize a distribution of the same dimension as ω .

7 Experiments

7.1 Toolkit

To enable experiments on data, we implement ProDAG in a Julia (Bezanson et al., 2017) toolkit, built using the machine learning library Flux (Innes et al., 2018). Our toolkit handles linear and nonlinear DAGs and rapidly performs projections using parallel (batched CUDA) implementations of the projection algorithms. It is publicly available as an open source package on GitHub at

<https://github.com/ryan-thompson/ProDAG.jl>.

7.2 Synthetic data

Our method ProDAG is benchmarked against DAGMA (Bello et al., 2022), DiBS (Lorch et al., 2021), and BayesDAG (Annadani et al., 2023a). DAGMA is a frequentist version of our approach that delivers a point estimate DAG. DiBS and BayesDAG are state-of-the-art Bayesian approaches that learn posterior distributions over DAGs. Appendix D describes each method’s hyperparameters and implementation.

We consider several metrics that characterize different qualities of the learned posterior distributions. As a measure of uncertainty quantification, we report the Brier score under the posterior. As measures of structure recovery, we report the expected structural Hamming distance (SHD) and expected F1 score under the posterior. All three metrics compare the learned posterior to the ground truth DAG. Since DAGMA returns a single point estimate graph, the metrics are evaluated by taking its posterior as a Dirac delta distribution that places all mass on the learned graph. For ProDAG, DiBS, and DAGMA, the metrics are evaluated by drawing a sample of graphs from the learned posterior.

Figure 1 reports results on datasets simulated from linear DAGs. The sample size is varied between $n = 10$ and $n = 1000$ on a logarithmic scale, and the number of variables $p = 20$ (Figure 1a)

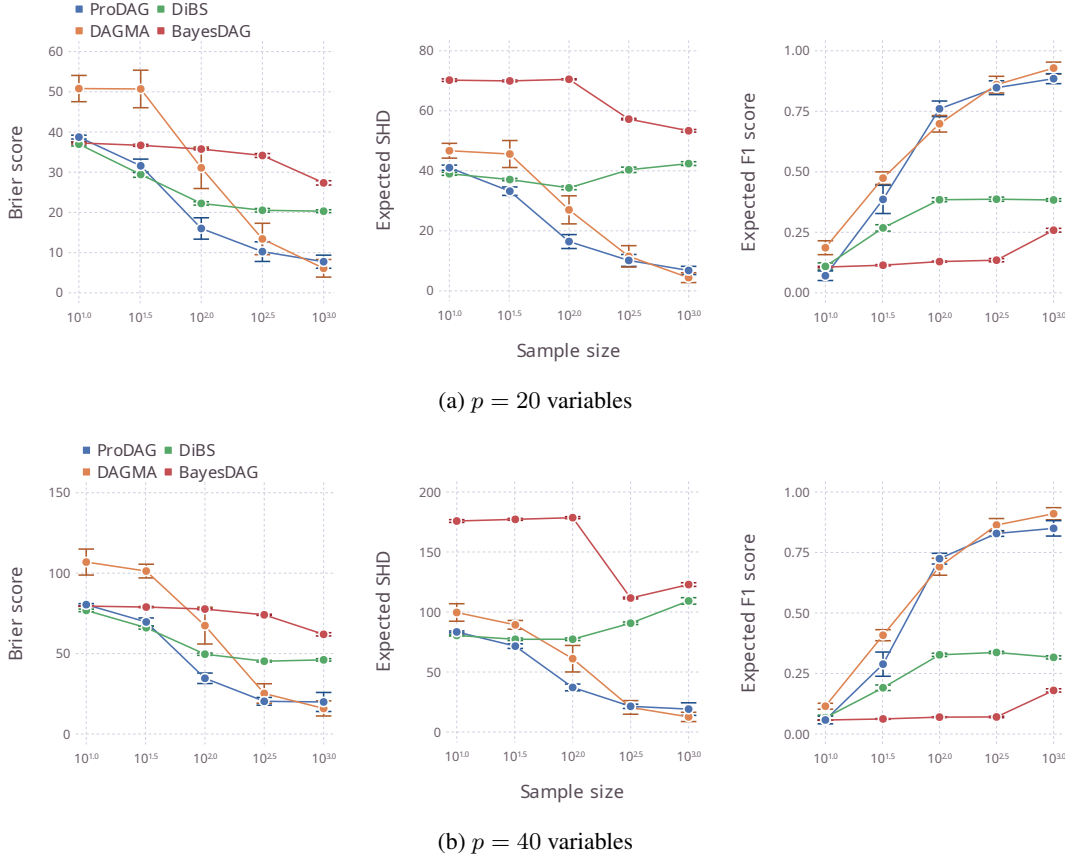


Figure 1: Performance as a function of the sample size n on synthetic data generated from *linear* DAGs. The number of variables $p \in \{20, 40\}$ and the number of edges is $2p$. The averages (solid points) and standard errors (error bars) are measured over 10 random datasets. Lower values of Brier score and expected SHD are better. Higher values of F1 score are better.

and $p = 40$ (Figure 1b). The number of ground truth edges is $2p$. Appendix E describes the full simulation design. ProDAG delivers highly competitive performance when the sample size is small to moderate, especially regarding uncertainty quantification (as measured by Brier score). For large sample sizes, where little uncertainty remains regarding the true graph, ProDAG is as competitive as the frequentist DAGMA. In contrast, DiBS and BayesDAG do not significantly improve as the sample size increases. Lorch et al. (2021) studied DiBS on a fixed sample size of $n = 100$, and their results approximately match ours at $n = 100$. Meanwhile, Annadani et al. (2023a) evaluated BayesDAG on linear DAGs of size $p = 5$, where the graphs are one to two orders of magnitude smaller than here.

Figure 2 reports results on datasets simulated from nonlinear DAGs. Following Zheng et al. (2020), each variable is generated from a single hidden-layer neural network whose inputs are that variable’s parents. The learning task is more statistically and computationally challenging here than in the linear setting, so we fix the number of variables $p = 10$. The number of ground truth edges is again $2p = 20$. ProDAG continues to deliver strong performance, especially with regard to uncertainty quantification. The various improvements of ProDAG over DAGMA, DiBS, and BayesDAG also persist here in terms of uncertainty quantification and structure recovery. The results for DiBS roughly match those in Lorch et al. (2021), where its expected SHD is approximately the same as the null model (a graph with no edges). Annadani et al. (2023a) studied BayesDAG on a sample size of $n = 5000$, much larger than here. ProDAG does not appear to require a sample of similar size for good inference.

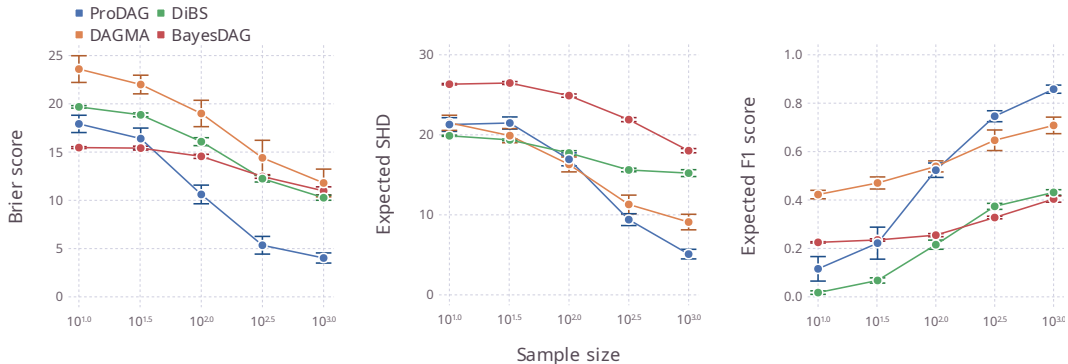


Figure 2: Performance as a function of the sample size n on synthetic data generated from *nonlinear* DAGs. The number of variables $p = 10$ and the number of edges is $2p$. The averages (solid points) and standard errors (error bars) are measured over 10 random datasets. Lower values of Brier score and expected SHD are better. Higher values of F1 score are better.

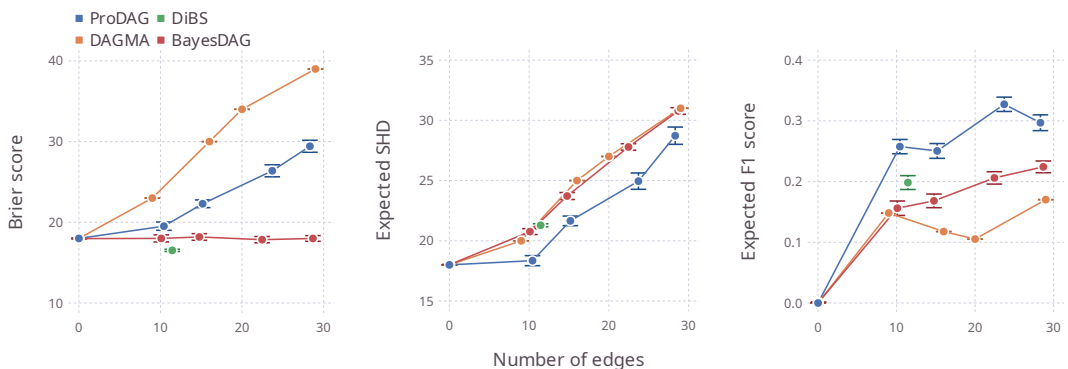


Figure 3: Performance as a function of the number of edges on the flow cytometry data. The averages (solid points) and standard errors (error bars) are measured over 10 different random seeds. Lower values of Brier score and expected SHD are better. Higher values of F1 score are better.

7.3 Real data

The flow cytometry data of [Sachs et al. \(2005\)](#) is a biological dataset designed to aid the discovery of protein signaling networks. The dataset, which contains $n = 7466$ human cell measurements on $p = 11$ phosphoproteins and phospholipids, is one of the few real datasets with an expert consensus graph available. This consensus graph, consisting of 18 directed edges, is taken to be the ground truth. Figure 3 reports the results on linear DAGs at several different sparsity levels. ProDAG uniformly improves on DAGMA. DiBS, which has no sparsity parameter and hence learns a graph at a single sparsity level, yields a competitive Brier score. BayesDAG also performs competitively with regard to Brier score, but underperforms ProDAG in terms of both expected SHD and expected F1-score.

8 Concluding remarks

DAGs are complex structures due to their acyclic nature, making Bayesian inference a formidable task, both statistically and computationally. This paper introduces ProDAG, a novel approach to the problem that employs projection-induced distributions that have support directly on the space of DAGs. We study some key properties of these distributions and demonstrate that they lead to accurate inference when used as a prior and approximate posterior in a variational framework. As an important extension, our approach generalizes to accommodate nonlinear DAGs, widening its applicability to a diverse range of problems and data. Our toolkit for ProDAG is publicly available on [GitHub](#).

References

- Yashas Annadani, Jonas Rothfuss, Alexandre Lacoste, Nino Scherrer, Anirudh Goyal, Yoshua Bengio, and Stefan Bauer. Variational causal networks: Approximate Bayesian inference over causal structures, 2021. arXiv: 2106.07635.
- Yashas Annadani, Nick Pawlowski, Joel Jennings, Stefan Bauer, Cheng Zhang, and Wenbo Gong. BayesDAG: Gradient-based posterior inference for causal discovery. In *Advances in Neural Information Processing Systems*, volume 36, pages 1738–1763, 7 2023a.
- Yashas Annadani, Panagiotis Tigas, Desi R Ivanova, Andrew Jesson, Yarin Gal, Adam Foster, and Stefan Bauer. Differentiable multi-target causal Bayesian experimental design. In *Proceedings of the 40th International Conference on Machine Learning*, volume 202, pages 34263–34279, 2023b.
- Kevin Bello, Bryon Aragam, and Pradeep Ravikumar. DAGMA: Learning DAGs via M-matrices and a log-determinant acyclicity characterization. In *Advances in Neural Information Processing Systems*, volume 35, pages 8226–8239, 2022.
- Jeff Bezanson, Alan Edelman, Stefan Karpinski, and Viral B Shah. Julia: A fresh approach to numerical computing. *SIAM Review*, 59:65–98, 2017.
- David M Blei, Alp Kucukelbir, and Jon D McAuliffe. Variational inference: A review for statisticians. *Journal of the American Statistical Association*, 112:859–877, 2017.
- Edwin V Bonilla, Pantelis Elinas, He Zhao, Maurizio Filippone, Vassili Kitsios, and Terry O’Kane. Variational DAG estimation via state augmentation with stochastic permutations, 2024. arXiv: 2402.02644.
- Bertrand Charpentier, Simon Kibler, and Stephan Günnemann. Differentiable DAG sampling. In *International Conference on Learning Representations*, 2022.
- Chris Cundy, Aditya Grover, and Stefano Ermon. BCD Nets: Scalable variational approaches for Bayesian causal discovery. In *Advances in Neural Information Processing Systems*, volume 34, pages 7095–7110, 2021.
- Tristan Deleu, Mizu Nishikawa-Toomey, Jithendaraa Subramanian, Nikolay Malkin, Laurent Charlin, and Yoshua Bengio. Joint Bayesian inference of graphical structure and parameters with a single generative flow network. In *Advances in Neural Information Processing Systems*, volume 36, pages 31204–31231, 2023.
- Chang Deng, Kevin Bello, Bryon Aragam, and Pradeep Ravikumar. Optimizing NOTEARS objectives via topological swaps. In *Proceedings of the 40th International Conference on Machine Learning*, volume 202, pages 7563–7595, 2023.
- John Duchi, Shai Shalev-Shwartz, Yoram Singer, and Tushar Chandra. Efficient projections onto the ℓ_1 -ball for learning in high dimensions. In *Proceedings of the 25th International Conference on Machine Learning*, pages 272–279, 2008.
- E Michael Foster. Causal inference and developmental psychology. *Developmental Psychology*, 46: 1454–1480, 2010.
- Tomas Geffner, Javier Antoran, Adam Foster, Wenbo Gong, Chao Ma, Emre Kiciman, Amit Sharma, Angus Lamb, Martin Kukla, Agrin Hilmkil, Joel Jennings, Nick Pawlowski, Miltiadis Allamanis, and Cheng Zhang. Deep end-to-end causal inference. In *NeurIPS 2022 Workshop on Causal Machine Learning for Real-World Impact*, 2022.
- Pierre Gillot and Pekka Parviainen. Learning large DAGs by combining continuous optimization and feedback arc set heuristics. In *Proceedings of the AAAI Conference on Artificial Intelligence*, volume 36, pages 6713–6720, 2022.
- Guido W Imbens. Potential outcome and directed acyclic graph approaches to causality: Relevance for empirical practice in economics. *Journal of Economic Literature*, 58:1129–1179, 2020.

- Michael J Innes, Elliot Saba, Keno Fischer, Dhairya Gandhi, Marco Concetto Rudilosso, Neethu Mariya Joy, Tejan Karmali, Avik Pal, and Viral B Shah. Fashionable modelling with Flux. In *Workshop on Systems for ML and Open Source Software at NeurIPS 2018*, 2018.
- Diederik P Kingma and Jimmy Lei Ba. Adam: A method for stochastic optimization. In *International Conference on Learning Representations*, 2015.
- Diederik P Kingma and Max Welling. Auto-encoding variational Bayes. In *International Conference on Learning Representations*, 2014.
- Neville Kenneth Kitson, Anthony C Constantinou, Zhigao Guo, Yang Liu, and Kiattikun Chobtham. A survey of Bayesian network structure learning. *Artificial Intelligence Review*, 56:8721–8814, 2023.
- S L Lauritzen and D J Spiegelhalter. Local computations with probabilities on graphical structures and their application to expert systems. *Journal of the Royal Statistical Society: Series B (Methodological)*, 50:157–224, 1988.
- Lars Lorch, Jonas Rothfuss, Bernhard Schölkopf, and Andreas Krause. DiBS: Differentiable Bayesian structure learning. In *Advances in Neural Information Processing Systems*, volume 34, pages 24111–24123, 2021.
- Hasan Manzour, Simge Küçükyavuz, Hao-Hsiang Wu, and Ali Shojaie. Integer programming for learning directed acyclic graphs from continuous data. *INFORMS Journal on Optimization*, 3: 46–73, 2021.
- Ignavier Ng, AmirEmad Ghassami, and Kun Zhang. On the role of sparsity and DAG constraints for learning linear DAGs. In *Advances in Neural Information Processing Systems*, volume 33, pages 17943–17954, 2020.
- Trevor Park and George Casella. The Bayesian lasso. *Journal of the American Statistical Association*, 103:681–686, 2008.
- Judea Pearl. *Probabilistic Reasoning in Intelligent Systems*. Morgan Kaufmann, San Francisco, USA, 1988.
- Judea Pearl. *Causality: Models, Reasoning, and Inference*. Cambridge University Press, New York, USA, 2nd edition, 2009.
- Karen Sachs, Omar Perez, Dana Pe’er, Douglas A Lauffenburger, and Garry P Nolan. Causal protein-signaling networks derived from multiparameter single-cell data. *Science*, 308:523–529, 2005.
- Peter W G Tennant, Eleanor J Murray, Kellyn F Arnold, Laurie Berrie, Matthew P Fox, Sarah C Gadd, Wendy J Harrison, Claire Keeble, Lysie R Ranker, Johannes Textor, Georgia D Tomova, Mark S Gilthorpe, and George T H Ellison. Use of directed acyclic graphs (DAGs) to identify confounders in applied health research: Review and recommendations. *International Journal of Epidemiology*, 50:620–632, 2021.
- Ryan Thompson, Edwin V Bonilla, and Robert Kohn. Contextual directed acyclic graphs. In *Proceedings of the 27th International Conference on Artificial Intelligence and Statistics*, volume 238, pages 2872–2880, 2024.
- Matthew J Vowels, Necati Cihan Camgoz, and Richard Bowden. D’ya like DAGs? A survey on structure learning and causal discovery. *ACM Computing Surveys*, 55:1–36, 2022.
- Benjie Wang, Matthew Wicker, and Marta Kwiatkowska. Tractable uncertainty for structure learning. In *Proceedings of the 39th International Conference on Machine Learning*, volume 162, pages 23131–23150, 2022.
- Maoran Xu and Leo L Duan. Bayesian inference with the l_1 -ball prior: Solving combinatorial problems with exact zeros. *Journal of the Royal Statistical Society: Series B (Statistical Methodology)*, 85:1538–1560, 2023.

- Maoran Xu, Hua Zhou, Yujie Hu, and Leo L Duan. Bayesian inference using the proximal mapping: Uncertainty quantification under varying dimensionality. *Journal of the American Statistical Association*, 2023.
- Yue Yu, Tian Gao, Naiyu Yin, and Qiang Ji. DAGs with no curl: An efficient DAG structure learning approach. In *Proceedings of the 38th International Conference on Machine Learning*, volume 139, pages 12156–12166, 2021.
- Ming Yuan and Yi Lin. Model selection and estimation in regression with grouped variables. *Journal of the Royal Statistical Society: Series B (Statistical Methodology)*, 68:49–67, 2006.
- Xun Zheng, Bryon Aragam, Pradeep Ravikumar, and Eric P Xing. DAGs with NO TEARS: Continuous optimization for structure learning. In *Advances in Neural Information Processing Systems*, volume 31, 2018.
- Xun Zheng, Chen Dan, Bryon Aragam, Pradeep Ravikumar, and Eric P Xing. Learning sparse nonparametric DAGs. In *Proceedings of the 23rd International Conference on Artificial Intelligence and Statistics*, volume 108, pages 3414–3425, 2020.

A Proof of Theorem 1

Proof. We proceed by proving the each claim of the theorem in turn.

Uniqueness We begin by proving the first claim that the projection is unique almost surely. First, observe that the weighted adjacency matrix W can be expressed in terms of an adjacency matrix S and a continuous matrix V :

$$\min_{W \in \text{DAG}, \|W\|_{\ell_1} \leq \lambda} \|\tilde{W} - W\|_F^2 \iff \min_{\substack{S \in \{0,1\}^{p \times p}, S \in \text{DAG} \\ V \in \mathbb{R}^{p \times p}, \|V\|_{\ell_1} \leq \lambda}} f_S(V; \tilde{W}) := \|\tilde{W} - S \odot V\|_F^2,$$

where \odot denotes the Hadamard product and we adopt the convention that $v_{jk} = 0$ if $s_{jk} = 0$. We can write the minimization on the right-hand side as a min-min problem:

$$\min_{\substack{S \in \{0,1\}^{p \times p}, S \in \text{DAG} \\ V \in \mathbb{R}^{p \times p}, \|V\|_{\ell_1} \leq \lambda}} f_S(V; \tilde{W}) \iff \min_{S \in \{0,1\}^{p \times p}, S \in \text{DAG}} \min_{V \in \mathbb{R}^{p \times p}, \|V\|_{\ell_1} \leq \lambda} f_S(V; \tilde{W}).$$

Consider the inner optimization problem on the right-hand side. Let V^* denote an optimal solution to this problem, and define the set of non-unique solutions as

$$A_S := \{\tilde{W} \in \mathbb{R}^{p \times p} \mid f_S(V_1^*; \tilde{W}) = f_S(V_2^*; \tilde{W}), V_1^* \neq V_2^*\}.$$

Since $f_S(V; \tilde{W})$ is strictly convex in V and continuous and \tilde{W} , the optimal objective value $f_S(V^*; \tilde{W})$ is continuous and unique with respect to the measure on \tilde{W} . Hence, the set A_S has measure zero with respect to \tilde{W} . Now, define the set of non-unique solutions across any two different adjacency matrices S_1 and S_2 as

$$A_{S_1, S_2} := \{\tilde{W} \in \mathbb{R}^{p \times p} \mid f_{S_1}(V_1^*; \tilde{W}) = f_{S_2}(V_2^*; \tilde{W}), V_1^* \neq V_2^*\}.$$

Since S_1 and S_2 simply induce different subspaces over \tilde{W} , the set A_{S_1, S_2} also has measure zero. Moreover, the union of A_{S_1, S_2} over all adjacency matrices $S_1 \neq S_2$ has measure zero. We conclude that the projection is unique almost surely.

Measurability To prove the second claim that the projection is measurable, define the functions

$$g_\lambda(\tilde{W}, S) := \arg \min_{\substack{V \in \mathbb{R}^{p \times p} \\ \|V\|_{\ell_1} \leq \lambda}} \|\tilde{W} - S \odot V\|_F^2,$$

and

$$h_\lambda(\tilde{W}) := \arg \min_{\substack{S \in \{0,1\}^{p \times p} \\ S \in \text{DAG}}} \|\tilde{W} - S \odot g_\lambda(\tilde{W}, S)\|_F^2.$$

It follows that

$$\text{proj}_\lambda(\tilde{W}) = g_\lambda(\tilde{W}, h_\lambda(\tilde{W})).$$

We now demonstrate that each of these functions are measurable in \tilde{W} . First, for fixed S , the function $g_\lambda(\tilde{W}, S)$ is the minimizing argument of a convex optimization problem and hence continuous in \tilde{W} . Continuous functions are measurable with respect to their argument, and therefore $g_\lambda(\tilde{W}, S)$ is measurable in \tilde{W} . Second, since the set of acyclic adjacency matrices is finite, the function $h_\lambda(\tilde{W})$ takes the pointwise minimum of finitely many measurable functions and returns the adjacency matrix indexed by that minimum. A pointwise minimum of measurable functions is itself measurable. Lastly, since $g_\lambda(\tilde{W}, S)$ and $h_\lambda(\tilde{W})$ are both measurable in \tilde{W} , their composition $g_\lambda(\tilde{W}, h_\lambda(\tilde{W}))$ must also be measurable in \tilde{W} . We conclude that $\text{proj}_\lambda(\tilde{W})$ is measurable in \tilde{W} . \square

B Proof of Theorem 2

Proof. Let W^* denote an optimal solution to projection (3). The KKT conditions for stationarity and complementary slackness are

$$\partial \left(\frac{1}{2} \|\tilde{W} - W^*\|_F^2 + \nu^* (\|W^*\|_{\ell_1} - \lambda) + \eta^* h(W^*) \right) \ni 0 \quad (8)$$

and

$$\nu^*(\|W^*\|_{\ell_1} - \lambda) = 0, \quad (9)$$

where ν^* and η^* are the optimal values of the KKT multipliers. The optimal solution W^* is implicitly a function of the problem data \tilde{W} and λ , i.e., $W^* = W^*(\tilde{W}, \lambda)$, as are the optimal KKT multipliers $\nu^* = \nu^*(\tilde{W}, \lambda)$ and $\eta^* = \eta^*(\tilde{W}, \lambda)$. Denote the set of nonzeros by \mathcal{A} .

Non-binding ℓ_1 constraint Suppose the ℓ_1 constraint is non-binding. Evaluating the subderivative on the left-hand side of the stationarity condition (8) gives

$$w_{jk}^* - \tilde{w}_{jk} = 0,$$

where we use that $\nu^* = 0$ and $\partial h(W^*)/\partial w_{jk}^* = 0$. Differentiating this expression with respect to \tilde{w}_{qr} for $(j, k) \in \mathcal{A}$, gives

$$\frac{\partial w_{jk}^*}{\partial \tilde{w}_{qr}} = \delta_{jk}^{qr}.$$

For those $(j, k) \notin \mathcal{A}$, $w_{jk}^* = 0$ and hence

$$\frac{\partial w_{jk}^*}{\partial \tilde{w}_{qr}} = 0.$$

Moreover, because $\nu^* = 0$, we have

$$\frac{\partial w_{jk}^*}{\partial \lambda} = 0$$

for all (j, k) .

Binding ℓ_1 constraint - Active set Suppose the ℓ_1 constraint is binding and consider the gradients for w_{jk}^* in the active set. For these $(j, k) \in \mathcal{A}$, it follows from the stationarity condition (8) that

$$w_{jk}^* - \tilde{w}_{jk} + \nu^* \text{sign}(w_{jk}^*) = 0, \quad (10)$$

where we again use that $\partial h(W^*)/\partial w_{jk}^* = 0$. The complementary slackness condition (9) for $(j, k) \in \mathcal{A}$ gives

$$\sum_{(j,k) \in \mathcal{A}} |w_{jk}^*| - \lambda = 0. \quad (11)$$

We proceed by first deriving the gradients of w_{jk}^* with respect to \tilde{w}_{qr} . Differentiating (10) with respect to \tilde{w}_{qr} gives

$$\frac{\partial w_{jk}^*}{\partial \tilde{w}_{qr}} - \delta_{jk}^{qr} + \frac{\partial \nu^*}{\partial \tilde{w}_{qr}} \text{sign}(w_{jk}^*) + \nu^* \frac{\partial}{\partial \tilde{w}_{qr}} \text{sign}(w_{jk}^*) = 0,$$

from which it follows

$$\frac{\partial w_{jk}^*}{\partial \tilde{w}_{qr}} = \delta_{jk}^{qr} - \frac{\partial \nu^*}{\partial \tilde{w}_{qr}} \text{sign}(w_{jk}^*). \quad (12)$$

Next, differentiating (11) with respect to \tilde{w}_{qr} gives

$$\sum_{(j,k) \in \mathcal{A}} \text{sign}(w_{jk}^*) \frac{\partial w_{jk}^*}{\partial \tilde{w}_{qr}} = 0. \quad (13)$$

Substituting (12) into (13) and solving for $\partial \nu^*/\partial \tilde{w}_{qr}$ yields

$$\frac{\partial \nu^*}{\partial \tilde{w}_{qr}} = \frac{\text{sign}(w_{qr}^*)}{\sum_{(j,k) \in \mathcal{A}} \text{sign}(w_{jk}^*)^2} = \frac{1}{|\mathcal{A}|} \text{sign}(w_{qr}^*). \quad (14)$$

Finally, substituting (14) back into (12) gives

$$\frac{\partial w_{jk}^*}{\partial \tilde{w}_{qr}} = \delta_{jk}^{qr} - \frac{\text{sign}(w_{qr}^*) \text{sign}(w_{jk}^*)}{|\mathcal{A}|}.$$

We turn now to the gradients of w_{jk}^* with respect to λ . Differentiating (10) with respect to λ gives

$$\frac{\partial w_{jk}^*}{\partial \lambda} + \frac{\partial \nu^*}{\partial \lambda} \text{sign}(w_{jk}^*) + \nu^* \frac{\partial}{\partial \lambda} \text{sign}(w_{jk}^*) = 0,$$

from which it follows

$$\frac{\partial w_{jk}^*}{\partial \lambda} = -\frac{\partial \nu^*}{\partial \lambda} \text{sign}(w_{jk}^*). \quad (15)$$

Next, differentiating (11) with respect to λ gives

$$\sum_{(j,k) \in \mathcal{A}} \text{sign}(w_{jk}^*) \frac{\partial w_{jk}^*}{\partial \lambda} - 1 = 0. \quad (16)$$

Substituting (15) into (16) and solving for $\partial \nu^* / \partial \lambda$ yields

$$\frac{\partial \nu^*}{\partial \lambda} = -\frac{1}{|\mathcal{A}|}. \quad (17)$$

Finally, substituting (17) back into (15) gives

$$\frac{\partial w_{jk}^*}{\partial \lambda} = \frac{\text{sign}(w_{jk}^*)}{|\mathcal{A}|}.$$

Binding ℓ_1 constraint - Inactive set Suppose the ℓ_1 constraint is binding and consider the gradients for w_{jk}^* in the inactive set. These $(j, k) \notin \mathcal{A}$ play no role in either of the KKT conditions, and hence have no gradient with respect to \tilde{w}_{jk} or λ :

$$\frac{\partial w_{jk}^*}{\partial \tilde{w}_{qr}} = 0$$

and

$$\frac{\partial w_{jk}^*}{\partial \lambda} = 0.$$

□

C Proof of Proposition 1

Proof. The acyclicity constraints forces $\|\omega_{jk}^h\| = 0$ for some j and k , meaning the whole vector $\omega_{jk}^h = 0$. Likewise, the sparsity constraint, which represents a group lasso regularizer (Yuan and Lin, 2006), is also known to set some ω_{jk}^h to zero. Those surviving vectors that are not set to zero are shrunk towards zero by an amount $\|\omega_{jk}^h\| / \|\tilde{\omega}_{jk}^h\|$. The combined effect of these two constraints gives that

$$\omega_{jk}^h = \tilde{\omega}_{jk}^h \frac{\|\omega_{jk}^h\|}{\|\tilde{\omega}_{jk}^h\|},$$

which equals zero if $\|\omega_{jk}^h\|_2 = 0$. Now, observe that the objective function can be expressed solely in terms of the norms of each vector:

$$\begin{aligned} \sum_{j,k} \|\tilde{\omega}_{jk}^h - \omega_{jk}^h\|^2 &= \sum_{j,k} \left\| \tilde{\omega}_{jk}^h - \tilde{\omega}_{jk}^h \frac{\|\omega_{jk}^h\|}{\|\tilde{\omega}_{jk}^h\|} \right\|^2 \\ &= \sum_{j,k} \left\| \tilde{\omega}_{jk}^h \left(1 - \frac{\|\omega_{jk}^h\|}{\|\tilde{\omega}_{jk}^h\|} \right) \right\|^2 \\ &= \sum_{j,k} \|\tilde{\omega}_{jk}^h\|^2 \left(1 - \frac{\|\omega_{jk}^h\|}{\|\tilde{\omega}_{jk}^h\|} \right)^2 \\ &= \sum_{j,k} (\|\tilde{\omega}_{jk}^h\| - \|\omega_{jk}^h\|)^2. \end{aligned}$$

Taking $\tilde{w}_{jk} = \|\tilde{\omega}_{jk}^h\|$ and $w_{jk} = \|\omega_{jk}^h\|$ yields the claim of the proposition.

□

D Implementation

ProDAG uses a multivariate Gaussian prior on \tilde{W} with independent elements, each having mean zero and variance one. The variational posterior on \tilde{W} is also taken as a multivariate Gaussian with independent elements, where the means and variances are initialized at their prior values. We use the Adam optimizer (Kingma and Ba, 2015) with a learning rate of 0.1 to minimize the variational objective function. The posterior variances are held positive during optimization using a softplus transform. At each Adam iteration, 1000 samples of \tilde{W} are drawn from the posterior to estimate the objective function. To project these sampled \tilde{W} and obtain W , we solve the projection using gradient descent with learning rates of $1/p$ and $0.25/p$ for the linear and nonlinear settings, respectively.

For the benchmark methods, we use the respective authors’ open-source Python implementations:

- DAGMA: <https://github.com/kevinsbello/dagma>, v1.1.0, Apache License 2.0;
- DiBS: <https://github.com/larslorch/dibs>, v1.3.3, MIT License; and
- BayesDAG: <https://github.com/microsoft/Project-BayesDAG>, v0.1.0, MIT License.

We use 50 particles for DiBS’s particle variational inference. More particles lead to out-of-memory. The sparsity parameter λ of each method is tuned over a grid of 10 values between λ^{\min} and λ^{\max} .⁶

- ProDAG: $\lambda^{\min} = 0$ and $\lambda^{\max} = p$ (linear setting) or $\lambda^{\max} = 3p$ (nonlinear setting);
- DAGMA: $\lambda^{\min} = 10^{-3}$ and $\lambda^{\max} = 1$;
- DiBS: does not include a sparsity parameter; and
- BayesDAG: $\lambda^{\min} = 10$ and $\lambda^{\max} = 10^3$

The grids are chosen so that the learned sparsity level matches the true sparsity level for some value between λ^{\min} and λ^{\max} . For ProDAG and DAGMA, we choose λ from the grid using a separate validation set of size $\lfloor 0.1n \rfloor$. In the nonlinear setting, DAGMA’s Python implementation does not return the neural network (only its weighted adjacency matrix), so we could not use validation tuning and instead choose its λ by revealing the true sparsity level. Similarly, we could not extract the models from BayesDAG (only samples of binary adjacency matrices), so we also choose its λ by revealing the true sparsity level.

In the nonlinear setting, the neural networks for ProDAG and DiBS consist of a single hidden layer with 10 neurons that use ReLU activation functions. DAGMA employs the same architecture but the neurons use sigmoid activation functions (its implementation does not support custom activation functions). The network for BayesDAG consists of two hidden layers, each with 128 neurons (its implementation does not support custom numbers of layers or neurons) that use ReLU activation functions.

The experiments are run on a Linux workstation with an AMD Ryzen Threadripper 3970x CPU, 128GB RAM, and two NVIDIA GeForce RTX 4090 GPUs. Individual experiments are run on either a single GPU or a single CPU core. The total run time for all experiments is less than 24 hours.

E Simulation design

The synthetic datasets generated from linear DAGs are constructed as follows. We first randomly sample an Erdős–Rényi graph with p nodes and $2p$ edges. The edges of this undirected graph are then oriented according to a randomly generated topological ordering. Each directed edge in the graph is then weighted by sampling weights uniformly on the interval $[0.3, 0.7]$, yielding a weighted adjacency matrix W . We then draw the noise $\varepsilon_1, \dots, \varepsilon_n$ iid as $N(0, I)$ and finally generate the variables as

$$x_i = W^\top x_i + \varepsilon_i, \quad i = 1, \dots, n.$$

⁶The parameter λ in ProDAG refers to the ℓ_1 ball size, whereas λ in DAGMA and BayesDAG refers to the coefficient on the ℓ_1 penalty.

For synthetic datasets generated from nonlinear DAGs, we first sample an Erdős–Rényi graph and orientate it according to a random topological ordering. We then generate a feedforward neural network f_k with a single hidden layer of 10 neurons for $k = 1, \dots, p$. The weights of f_k are sampled uniformly from $[0.3, 0.7]$, with hidden layer weights of node k 's non-parents set to zero. The activation is a ReLU. The noise $\varepsilon_1, \dots, \varepsilon_n$ is drawn iid as $N(0, I)$ and the variables are generated as

$$x_i = f(x_i) + \varepsilon_i, \quad i = 1, \dots, n,$$

where $f(x) = (f_1(x), \dots, f_p(x))$.

F Limitations

Though our approach has several favorable properties, it naturally has limitations, the main ones we highlight here. As with most Bayesian approaches that employ variational inference, ours does not guarantee that the learned variational posterior approximates the true posterior well. The possibility of a poor variational approximation is further complicated by the nonconvexity of the acyclicity constraint, giving rise to a nonconvex optimization problem that can be solved only to a stationary point. We remark, however, that nonconvexity is true of most existing DAG learning methods.

G Societal impacts

DAG learning tools play a key role in causal inference, where the goal is to establish causal relationships between random variables. Our approach benefits from quantifying uncertainty in this process, which can help guide downstream decision-making. However, as with any DAG learning tool applied to observational data, one cannot causally interpret the DAGs learned by our approach without making empirically unverifiable assumptions such as causal sufficiency. Therefore, it is crucial to involve subject-matter experts capable of determining the validity of such assumptions.